Supporting Information

Cascade Amplification-Mediated In Situ Hot-Spot Assembly for MicroRNA Detection and Molecular Logic Gate Operations

Sha Yu,[†] Yingying Wang,[†] Li-Ping Jiang,*[†] Sai Bi,*[‡] and Jun-Jie Zhu[†]

[†]State Key Laboratory of Analytical Chemistry for Life Science, School of Chemistry and Chemical Engineering, Nanjing University, Nanjing, Jiangsu 210093, China

[‡]Collaborative Innovation Center for Marine Biomass Fiber, Materials and Textiles of Shandong Province, College of Chemistry and Chemical Engineering, Laboratory of Fiber Materials and Modern Textiles, the Growing Base for State Key Laboratory, Qingdao University, Qingdao 266071, PR China

E-mail: jianglp@nju.edu.cn, bisai11@126.com

Table of Contents

Additional Experimental Section

Materials. Tris (2-carboxyethyl) phosphine hydrochloride (TCEP), 6-mercapto-1-hexanol (MCH), and hexaammineruthenium(II) chloride ($[Ru(NH_3)_6]^{3+}$, RuHex) were purchased from Sigma Aldrich (St. Louis, MO). Indium tin oxide (ITO) electrodes (type JH52, ITO coating 3 ± 5 nm, resistance ≤ 10 Ω/square) were obtained from Nanjing Zhongjingkeyi Technology Co., Ltd. (China). TiO_2 powder (P25) was purchased from Degussa Co., Ltd. (Germany). Ascorbic acid (AA) and sodium dodecyl sulfonate were ordered from Sinopharm Chemical Reagent Co., Ltd. (China). 40% acrylamide mix solution, ammonium persulfate (APS), 1,2-bis(dimethylamino)-ethane (TEMED), and DNA ladder were obtained from Sangon Biotechnology Co., Ltd. (Shanghai, China). Duplex-specific nuclease (DSN) was ordered from Evrogen Joint Stock Company (Russa). The nucleic acids used in this work were synthesized and HPLC purified by Sangon Biotechnology Co., Ltd. (Shanghai, China). The sequences are listed in Table S1. The stock solution of each nucleic acid (10 mM) was prepared with TE buffer containing 10 mM Tris-HCl, 1 mM EDTA, 12.5 mM $MgCl_2$ (pH 7.4). The DNA hairpins (H1, H2, H3 and DP) were prepared by annealing at 90 ^oC for 5 min and slowly cooling to room temperature. Their secondary structures are shown in Figure S1. A Tris-HCl solution (10 mM, pH 7.4) containing $[Ru(NH_3)_6]^{3+}$ (5 μM) was used as the electrochemical buffer. A PBS buffer (0.1 M, pH 7.4) containing $Fe(CN)_6^{3+}/Fe(CN)_6^{4+}$ (10 mM) and KCl (1 M) was used as the electrochemical impedance spectroscopy (EIS) buffer. All the chemicals were of analytical grade and used as received without further purification. RNase-free water was used in all experiments.

Table S1. Oligonucleotides Sequences Used in This Study

Name	Sequence (5'-3')[a]
miR-141	UAACACUGUCUGGUAAAGAUGG
mismatched miR-141	UAACACUGUCUCGUAAAGAUGG
miR-21	UAGCUUAUCAGACUGAUGUUGA
miR-200a	UAACACUGUCUGGUAACGAUGU
miR-200b	UAAUACUGCCUGGUAAUGAUGA
miR-200c	UAAUACUGCCGGGUAAUGAUGGA
miR-429	UAAUACUGUCUGGUAAAACCGU
input 2 for INH	CUGUAAGUAGUGCGAGUUAG
H1	CAGTCTACCATCTTTACCAGACAGTGTTATAGACTGCTAACTCGCACTACTTACAG
H2	SH-CTAACTCGCACTACTTACGCTCAACTAGACTGCTGTAAGTAGTGCGAGTTAGCAGTCTA
H3	SH-ACGCTCAACTAGACTGCTAACTCGCACTACTTACAGCAGTCTAGTTGAGCGTAAGTAGT
DP	CAGTCTATCAACATCAGTCTGATAAGCTATAGACTGCTAACTCGCACTACTTACAGCCATCTT TACCAGACAGTGTTACTGTAGCGAG

The mismatched bases of miR-141 are underlined.

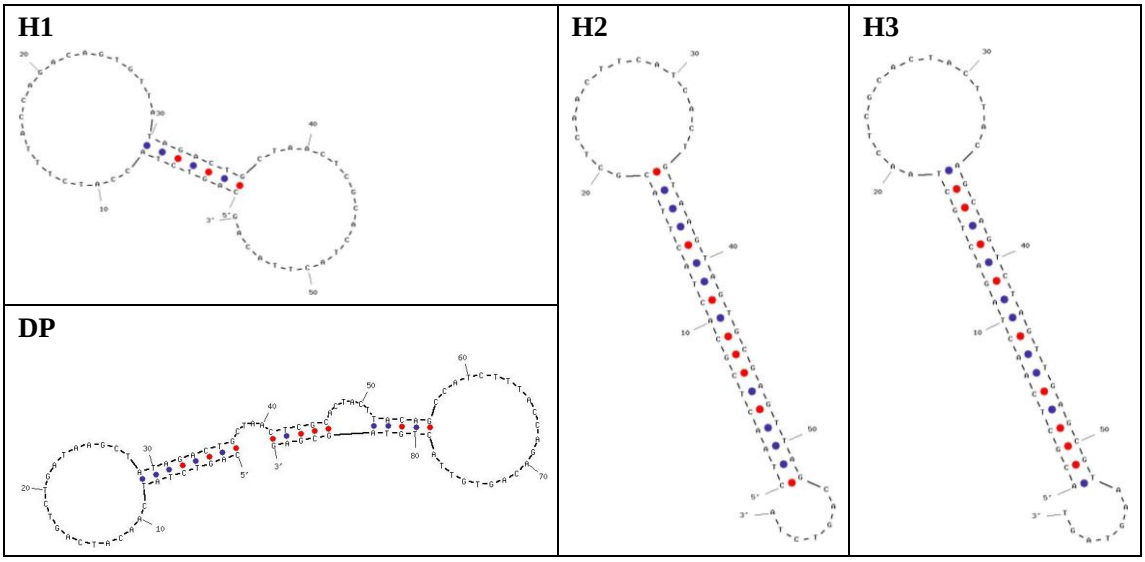

Figure S1. Secondary structures of DNA hairpins used in this study (www.idtdna.com).

Apparatus. The UV-Vis absorption spectra were obtained on a UV-Vis spectrometer UV-3600 (Shimadzu, Japan). Transmission electron microscopy (TEM) and scanning electron microscopy (SEM) were carried out on a JEOL-2010 transmission electron microscope (JEOL, Japan) and an S-4800 scanning electron microscope (Hitachi Co., Japan), respectively. High-resolution TEM

(HRTEM) images were performed using a JEM-2100 microscope (JEOL, Japan). Zeta potential was obtained on a ZEN2600 (Malvern Instruments Limited, England) and the dynamic light scattering (DLS) was obtained on a 90 plus (Brookhaven Instruments, USA). Fluorescence (FL) measurements were conducted on a RF-5301PC fluorescence spectrometer (Shimadzu Co. Japan) equipped with a xenon lamp. The polyacrylamide gel electrophoresis (PAGE) was imaged with BIO-RAD ChemiDoc XRs. The electrochemical measurements were performed on a CHI 660D workstation (CH Instruments Inc., Shanghai, China) using a conventional three-electrode system: a Ag/AgCl (3 M KCl) as the reference electrode, a Pt wire as the counter electrode, and the fabricated gold electrode as the working electrode. Photoelectrochemical measurements were performed on a home-made system. A 500 W xenon lamp (the spectrum ranging from 200 to 2500 nm) was used as the irradiation source with the light intensity of 400 $mW \cdot cm^{-2}$ that was estimated by a radiometer (Photoelectric Instrument Factory of Beijing Normal University, China). Photocurrent output was recorded on a CHI 660D electrochemical workstation with a three-electrode system: a saturated Ag/AgCl electrode as the reference electrode, a platinum wire as the counter electrode, and the modified ITO electrode with an area of 0.25 cm^2 as the working electrode. The reverse transcription of miRNAs and quantitative real-time PCR (qRT-PCR) experiments were carried out on a PTC-1148 PCR (Bio-Rad, USA.) and an ABI Prism 7300 qRT-PCR (ABI, USA.), respectively.

Cell Culture. Human breast cancer cell (MDA-MB-231), human cervical cancer cell lines (HeLa), human prostate carcinoma cell lines (22Rv1) and Human breast cancer cell (MCF-7) were obtained from the Cell Bank of Type Culture Collection of Chinese Academy of Sciences (Shanghai, China). 22Rv1 cells were cultured in RPMI medium 1640 supplemented with 10%

fetal bovine serum (FBS) and penicillin-streptomycin (100 U/mL) at 37 ^{o}C in a humidified 5% CO_2 incubator. HeLa and MCF-7 cells were respectively cultured in Dulbecco's modified Eagle medium (DMEM), supplemented with 10% FBS and penicillin-streptomycin (100 U/mL) at 37 ^{o}C in a humidified 5% CO_2 incubator. MDA-MB231 was cultured in L-15,supplemented with 10% FBS and penicillin-streptomycin (100 U/mL) at 37 ^{o}C in a humidified 5% CO_2 incubator. The cells were grown with fresh medium at 50 mm plastic-bottom dishes. Then, the cells were harvested by trypsinization, washed with fresh medium three times, and suspended in fresh medium for following studies.

Photoelectrochemical Detection of MiR-141. *Fabrication of CdS/TiO_2/ITO Electrode.* The ITO electrode was fabricated according to previous work.[S1] Before use, the ITO electrode was cleaned ultrasonically by acetone, NaOH (1 M) in water/ethanol mixture (1:1, v/v), and deionized water for 15 min in order, and then dried at 100 ^{o}C for 6 h. The TiO_2 powder (10 mg) was dispersed in 10 mL of deionized water ultrasonically, and 20 μL of the resultant white suspension (1 mg/mL) was scattered on the pretreated ITO electrode with a fixed area of 0.25 cm^2. After air drying, the electrode was annealed at 450 ^{o}C for 30 min in ambient air atmosphere and then naturally cooled to room temperature. The CdS quantum dots (QDs) were assembled by alternately immersing the TiO_2/ITO electrode into PDDA solution (1%) and CdS QDs solution for 10 min, respectively. This process was repeated four times to obtain the desired CdS/TiO_2/ITO electrode. It should be noted that the electrode was carefully washed with deionized water after each immersing step.

Fabrication of the Sensor. Typically, thiol-modified H2 was immobilized on the CdS/TiO_2/ITO electrode via Cd-S bond. Briefly, 20 μL of H2 (1 μM) was dropped on the CdS/TiO_2/ITO electrode and incubated for 24 h at room temperature. After rinsing with Tris-HCl buffer to remove unbound

H2, the ITO/TiO_2/CdS electrode was incubated with 20 μL of 1 mM MCH for 1 h to block the unbound active sites, followed by rinsing with Tris-HCl buffer thoroughly. Subsequently, the electrode was incubated with 10 μL of DSN-assisted reaction products and 20 μL of HP-AuNPs for 1 h at 37 ^{o}C. The resultant electrode was rinsed with Tris-HCl buffer for the following photoelectrochemical measurement.

Photoelectrochemical Measurement. The photoelectrochemical detection was performed at room temperature in Tris-HCl buffer (0.1 M, pH 7.4) containing ascorbic acid (AA) (0.1 M) that was served as a sacrificial electron donor during photocurrent test. Light excitation below 460 nm was utilized as irradiation source and was switched on and off every 10 s. No bias potential was applied to the system. The AA electrolyte was deaerated by bubbling N_2 for 15 min before photocurrent measurement.

Additional Results and Discussion.

Determination of Surface Coverage of H2 on Gold Electrode. A fluorescence method was used to determine the surface coverage of H2 on the gold electrode. The H2 was labeled with FAM at 3'-end and thiol at 5'-end (named as FAM-H2), which was further immobilized on the gold electrode according to the method of "Electrochemical Detection of miR-141" in "Experimental Section". Briefly, 200 μL of FAM-H2 (0.1 μM) was first treated with 0.2 μL of TCEP (10 mM, pH 5.2) for 1 h at room temperature to reduce residual disulfide bonds. Then, 50 μL of FAM-H2 (0.1 μM) was dropped onto the surface of gold electrode and incubated for 16 h at 4 ^{o}C. The solution containing the redundant FAM-H2 was removed from the gold electrode for fluorescence

measurement. The calibration curve of fluorescence intensity at 520 nm versus FAM-H2 concentration is shown in Figure S2.

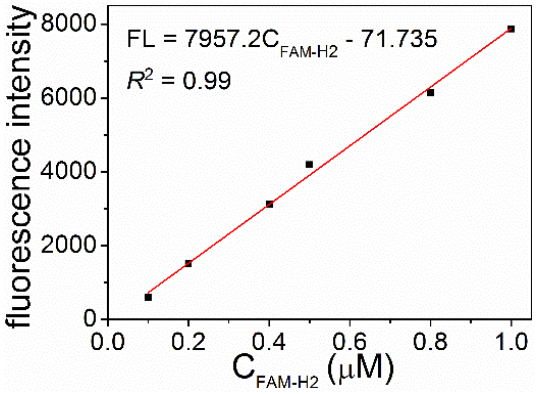

Figure S2. Calibration curve of fluorescence intensity at 520 nm versus FAM-H2 concentration.

The regression equation of Figure S2 is expressed as FL = 7957.2 C_{FAM-H2} -71.735 (R^2= 0.99).

The fluorescence intensity of the supernatant (50 μL) before immobilization is 677.83. → The concentration of FAM-H2 before immobilization is 94.2 nM.

The fluorescence intensity of the supernatant (50 μL) after immobilization is 566.43. → The concentration of FAM-H2 after immobilization is 80.2 nM.

Thus, the amounts of FAM-H2 immobilized on the gold electrode are (94.2 - 80.2) × 10^{-9} × 50 × 10^{-6} = 7.0 × 10^{-13} moles (0.7 pmol).

The surface coverage of H2 on the gold electrode is calculated to be 0.7 pmol with a diameter of 4.0 mm (~3.4 × 10^{10} copies/mm^2).

Determination of Surface Coverage of H2 and H3 on AuNPs. A 150 μL of thiol-labeled H3 (1.5 μM) was activated by 4.5 μL of TCEP (1 mM, pH 5.2) for 1 h and added into 150 μL of AuNPs. After incubation for 16 h at room temperature, the resulting colloid solution was salted

with 33 μL of NaCl (1 M) and allowed to stand for 24 h. Then, 300 μL of the supernatant was taken for UV-vis measurement. The amount of DNA hairpins immobilized on the AuNPs can be quantitatively calculated from the absorbance difference of H3 at 260 nm before and after immobilization. The calibration curve of UV-vis absorbance at 260 nm versus H3 concentration is shown in Figure S3.

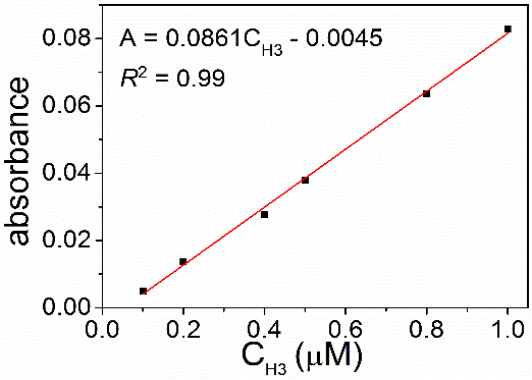

Figure S3. Calibration curve of UV-vis absorbance at 260 nm versus H3 concentration.

The regression equation of Figure S3 is expressed as $A = 0.0861C_{H3} - 0.0045$ (R^2= 0.99).

The UV-vis absorbance of the supernatant (300 μL) before immobilization is 0.12776. → The concentration of H3 before immobilization is 1.536 μM.

The UV-vis absorbance of the supernatant (300 μL) after immobilization is 0.09896. → The concentration of H3 after immobilization is 1.201 μM.

Thus, the amounts of total DNA hairpins immobilized on AuNPs are $(1.536 - 1.201) \times 10^{-6} \times 300 \times 10^{-6} = 1.005 \times 10^{-10}$ moles.

Then, 75 μL of FAM-H2 (1.5 μM) and 75 μL of H3 (1.5 μM) were activated by 2.25 μL of TCEP (10 mM, pH 5.2) for 1 h, respectively. The activated hairpins were mixed with 150 μL of

AuNPs. After incubation for 16 h at room temperature, the resulting colloid solution was salted with 33 μL of NaCl (1 M) and allowed to stand for 24 h. Then, 300 μL of supernatant was taken for fluorescence measurement. The amount of FAM-H2 immobilized on the AuNPs can be quantitatively calculated from the fluorescence intensity of FAM-H2 at 520 nm before and after immobilization.

The regression equation of Figure S2 is expressed as FL = 7957.2 C_{FAM-H2} -71.735 (R^2= 0.99).

The fluorescence intensity of the supernatant (300 μL) before immobilization is 5914.46. → Thus, the concentration of FAM-H2 before immobilization is 0.7523 μM.

The fluorescence intensity of the supernatant (300 μL) after immobilization is 4318.25. → Thus, the concentration of FAM-H2 after immobilization is 0.5517 μM

Thus, the amounts of FAM-H2 immobilized on AuNPs are (0.7523 - 0.5517) × 10^{-6} × 300 × 10^{-6} = 6.018 × 10^{-11} moles.

The extinction coefficient of 13 nm AuNPs at 520 nm is 2.7 × 10^{8} M^{-1}·cm^{-1}. Thus, the concentration of AuNPs solution is determined to be 4.2 nM by UV-vis measurement, and the amounts of AuNPs in 150 μL are 4.2 × 10^{-9} × 150 × 10^{-6} = 6.3 × 10^{-13} moles.

The ratio of H2 and H3 immobilized on AuNPs are shown in Table S2.

Table S2. Determination of Surface Coverage of H2 and H3 on AuNPs

AuNPs (moles)	total DNA (moles)	FAM-H2 (moles)	H3 (moles)	ratio of AuNPs/FAM-H2/H3
6.3 × 10^{-13}	1.005 × 10^{-10}	6.018 × 10^{-11}	4.032 × 10^{-11}	1/96/64

Reproducibility of H2-Immobilized Electrode.

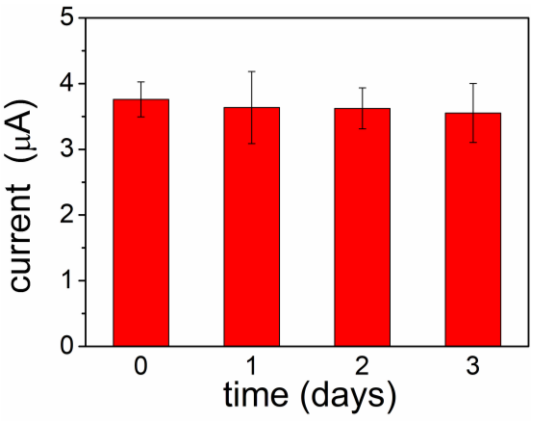

Figure S4. Reproducibility of the H2-immobilized electrodes stored for different days under 4 ^{o}C for the detection of connector DNA (0.1 nM). The error bars represent the standard deviations from three repetitive measurements.

Characterization of AuNP Probes.

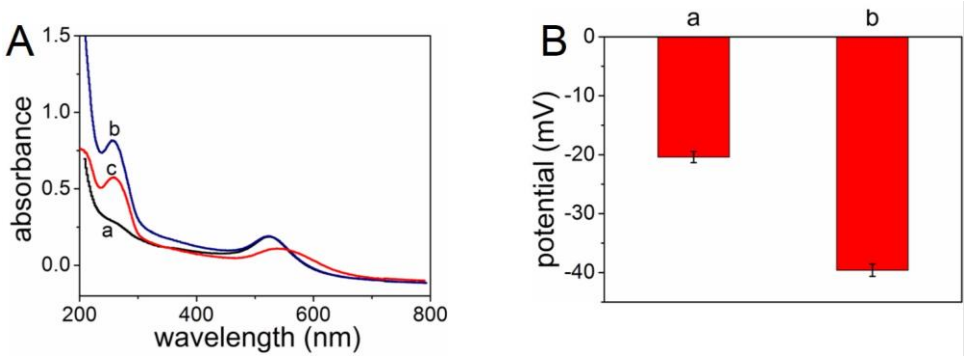

Figure S5. (A) UV-vis absorption spectra of (a) citrate-capped AuNPs (13 nm), (b) HP-AuNPs, and (c) HP-AuNPs incubated with connector DNAs (1 nM) for 1 h. (B) Zeta potential of (a) citrate-capped AuNPs (13 nm) and (b) HP-AuNPs. The error bars represent the standard deviations from three repetitive measurements.

Electrochemical Behaviors of Two Different Incubation Procedures.

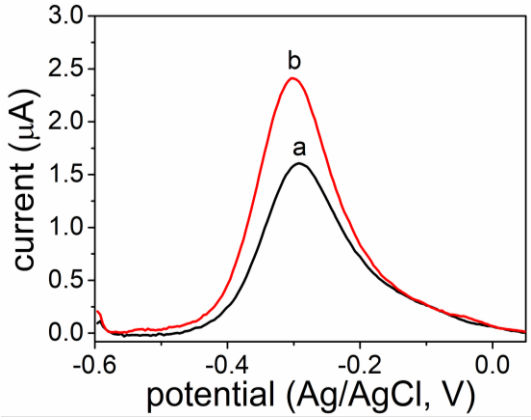

Figure S6. DPV curves of the gold electrodes treated with two different incubation procedures of (a) one-step method and (b) two-step method. For the one-step method, HP-AuNPs and connector DNAs are simultaneously introduced onto the H2-immobilized gold electrode. For the two-step method, connector DNAs are first introduced onto the H2-immobilized gold electrode for 1 h, and then HP-AuNPs are added to continue the reaction. The concentration of miR-141 is 5 pM.

Calculation of Detection Limit. In this assay, the calibration curve (inset of Figure 4A) can be divided into two linear segments with the regression equations as Y = 4.557 + 0.269logC (R^2 = 0.99, from 1 aM to 0.1 pM) and Y = 15.993 + 1.179logC (R^2 = 0.98, from 0.1 pM to 10 nM) (Figure S7).

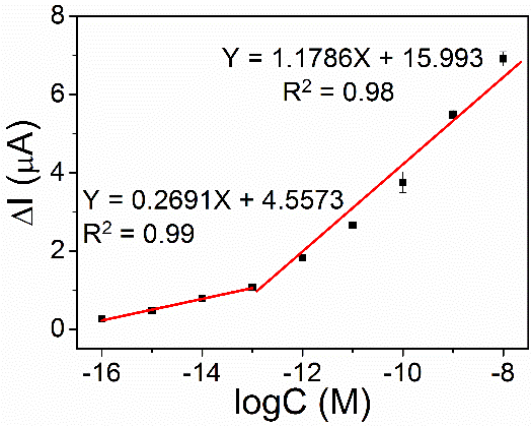

Figure S7. The calibration plots of the relative peak currents (ΔI) versus the logarithm of miR-141 concentrations. The error bars represent the standard deviations from three repetitive measurements.

The detection limit was calculated according to the literature using the linear segments at low concentrations from 1 aM to 0.1 pM as follows.[S2]

The calibration curve is plotted as:

$$Y = a + bX \qquad (1)$$

where a and b are the variables obtained by a least-squares linear regression of relative peak currents (ΔI, namely Y) versus the logarithm of miR-141 concentrations (logC, namely X).

From Figure S7, when the concentrations of miR-141 are in the range from 10 aM to 0.1 pM, the linear regression equation can be expressed as Y = 4.557 + 0.269logC (R^2 = 0.99). Thus, the a is corresponding to 4.557, the b is corresponding to 0.2691.

The b > 0,

$$A = \log I_0 + 3SD \qquad (2)$$

$$LOD = 10^{\frac{A-a}{b}} \qquad (3)$$

where SD is the standard deviation and I_0 is the peak current of the blank sample (without miR-141).

In this assay, SD = 0.4219, I_0 = 0.2291 μA, thus, A = 0.6257. Bring the A, a and b values into the formula (3), the LOD was calculated to be 25.1 aM.

Table S3. Comparison of DSN-Assisted Signal Amplification Assays for MiRNA Detection

Target	LOD	Method	Ref.
miR-141	100 fM	fluorescence	[S3]
miR-21	8 fM	fluorescence	[S4]
miR-141	1 pM	fluorescence	[S5]
miR-let-7a	0.4 pM	fluorescence	[S6]
miR-203	5 pM	fluorescence	[S7]
miR-let-7a	0.1 fM	colorimetry	[S8]
miR-let-7b	1.0 fM	electrochemistry	[S9]
miR-141	4.2 fM	electrochemistry	[S10]
miR-21	3.0 fM	electrochemistry	[S10]
miR-141	72.5 aM	electrochemistry	this work

Table S4. Comparison of Isothermal Amplification Strategies for Electrochemical Detection of MiRNAs

Amplification strategy	Target	LOD	Detection method	Ref.
Hybridization chain reaction (HCR) amplification	miR-let-7a	1 pM	DPV	[S11]
Combination of target recycling and cascade catalysis for signal amplification	miR-155	0.35 fM	DPV	[S12]
Combination of target-assisted polymerization nicking reaction and HCR	miR-199a	0.64 fM	DPV	[S13]
Isothermal exponential amplification reaction	miR-21	5.36 fM	DPV	[S14]
T7 exonuclease-assisted isothermal amplification	miR-let-7a	25 aM	DPV	[S15]
Combination of DSN-assisted target recycling amplification and CHA reaction	miR-141	25.1 aM	DPV	this work

Control Experiment Using Only H3-Modified AuNPs as Probes. The performance of the electrode using only H3-modified AuNPs as probes have been investigated. From Figure S8, the peak current of DPV gradually increases with the increase of miR-141 concentration from 0 to 100 nM. The detection limit is calculated to be 0.81 fM (S/N = 3), which is ~32-fold higher than that of the AuNP networks modified electrode. Thus, the proposed strategy of in situ self-assembly of AuNP networks on electrode via cascade amplification make a significant contribution to signal

amplification and the improvement of detection sensitivity.

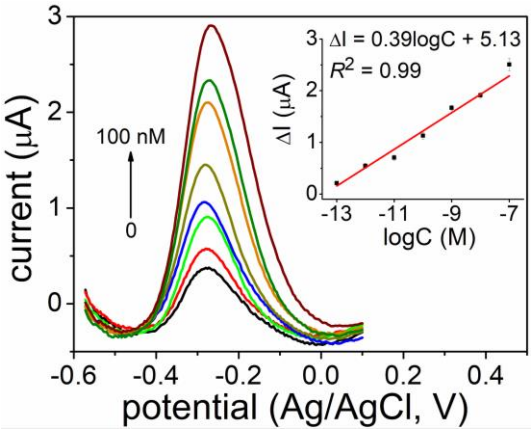

Figure S8. DPV curves of RuHeX using only H3-modified AuNPs as probes in response to different concentrations of miR-141. From bottom to top: 0, 100 fM, 1 pM, 10 pM, 100 pM, 1 nM, 10 nM and 100 nM. Inset: The corresponding calibration curve of the relative peak currents (ΔI) versus the logarithm of miR-141 concentrations. The error bars represent the standard deviations from three repetitive measurements.

Analytical Performance of Photoelectrochemical Biosensor. For photoelectrochemical detection, the CdS QDs were synthesized and characterized by high-resolution transmission electron microscopy (HRTEM), UV-vis absorption and fluorescence spectroscopy, respectively (Figure S9). HRTEM was performed to verify the morphology of the synthesized CdS QDs. As shown in Figure S9A, the lattice fringes as well as the outlines of CdS QDs can be clearly observed. The average size of CdS QDs is approximately 2.8 nm. The UV-vis absorption spectrum of CdS QDs exhibits a sharp absorption peak located at 362 nm (Figure S9B). In addition, a typical fluorescence emission peak is observed at 546 nm (Figure S9C), which is identical with the result reported in literature.[S16,S17] All the above results confirmed the successful preparation of CdS QDs.

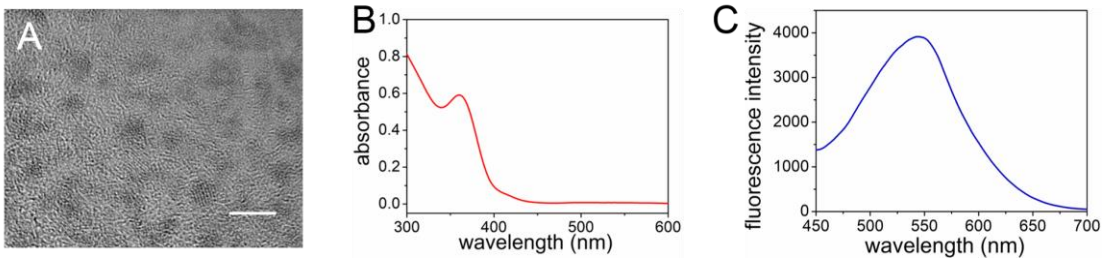

Figure S9. (A) HRTEM image, (B) UV-vis absorption and (C) fluorescence spectra of the prepared CdS QDs. Scale bar in (A): 5 nm.

Figure S10A illustrates the principle of the photoelectrochemical biosensor for the detection of miR-141 via cascade amplification for in situ self-assembly of AuNP networks on ITO electrode. The fabrication process of the photoelectrochemical biosensor was characterized as Figure S10B. The bare ITO electrode hardly has any photocurrent intensity (Figure S10B, curve a). After TiO_2 is deposited on the ITO, the electrode yields a relatively low photocurrent output (Figure S10B, curve b), since TiO_2 can only harvest the UV light, resulting in a low photocurrent conversion efficiency. After CdS QDs are coated on the ITO electrode, the photocurrent output obviously increases because of the efficient sensitization effect of CdS QDs (Figure S10B, curve c). However, the photocurrent intensity decreases after H2 and MCH are successively immobilized on the electrode (Figure S10B, curve d), which could be attributed to the weak charge-transfer ability of both H2 and MCH. After HP-AuNPs are bound on the electrode via DNA hybridization between H2 on the electrode and connector DNA, the photocurrent output is significantly weakened due to the activation of exciton energy transfer (EET) between CdS QDs and AuNPs (Figure S10B, curve e).[S18,S19] These results confirm the successful construction of the photoelectrochemical biosensor, which facilitates photoelectrochemical detection of miRNAs through self-assembly of AuNP networks on the electrode via cascade amplification in a

"signal-off" mode.

Subsequently, we investigated the photocurrent response of the proposed photoelectrochemical biosensor to different concentrations of miR-141. As illustrated in Figure S3C, the photocurrent signals gradually decrease with the increase of miR-141 concentrations. From the inset of Figure S10C, the relative photocurrent response linearly decreases with an increasing of the logarithm of miR-141 concentration in the range from 0 to 100 nM with a correlation coefficient of 0.99. The detection limit is calculated to be 35 fM (S/N = 3). Besides sensitivity, the selectivity of the photoelectrochemical biosensor was further investigated. In this assay, H1 is specific for miR-141, which thus exhibits an excellent selectivity to well-distinguish miR-141 from other miRNAs, even one-base mismatched miR-141 (Figure S10D). Therefore, our proposed photoelectrochemical biosensor demonstrates high selectivity for miRNA detection.

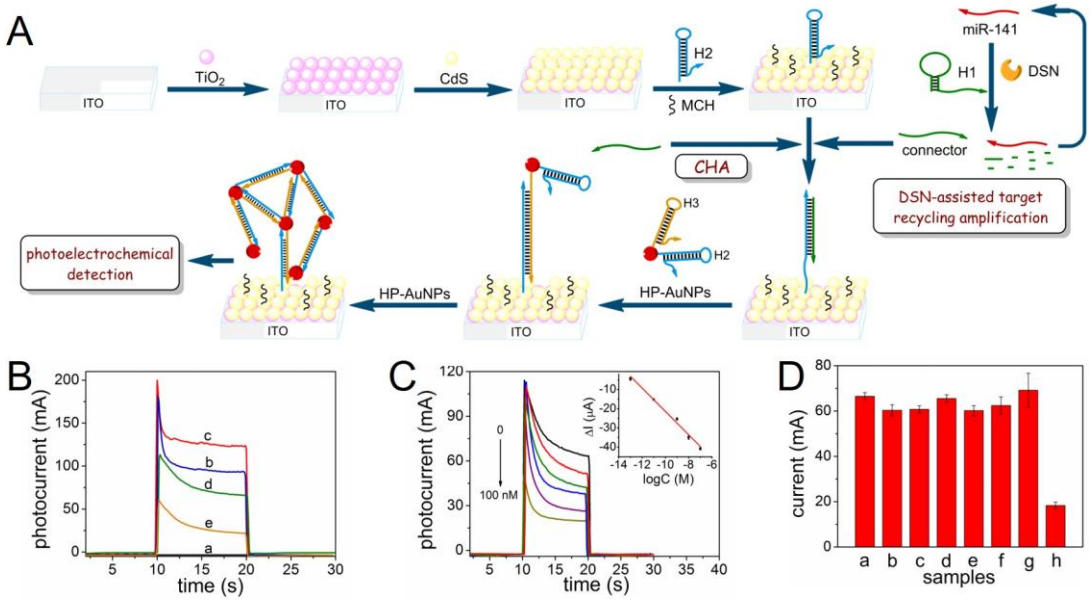

Figure S10. (A) Schematic illustration of cascade amplification of DSN-assisted target recycling and CHA reaction for in situ self-assembly of AuNP networks on electrode for label-free photoelectrochemical detection of miR-141 in "signal-off" mode. (B) Photocurrent responses of (a) ITO, (b) TiO_2/ITO, (c) CdS/TiO_2/ITO, (d) H2/MCH/CdS/TiO_2/ITO, and (e)

HP-AuNPs/H2/MCH/CdS/TiO_2/ITO in PBS buffer (pH 7.4) containing AA (0.1 M) as electron donor. (C) Photocurrent response of the proposed biosensor to different concentrations of miR-141. From top to bottom: 0, 0.1 pM, 10 pM, 1 nM, 10 nM, and 100 nM. Inset: The corresponding calibration curve of the relative photocurrents (ΔI) versus the logarithm of miR-141 concentrations. The error bars represent the standard deviations from three repetitive measurements. (D) Selectivity of the proposed photoelectrochemical biosensing platform towards (a) blank, (b) miR-21, (c) miR-200a (d) miR-200b (e) miR-200c (f) miR-429 (g) one base mismatched miR-141, and (h) miR-141. The concentration of miR-141 is 10 pM, while the concentrations of other miRNAs are 1 nM. The "blank" sample means the condition in the absence of any miRNA. The error bars represent the standard deviations from three repetitive measurements.

INH Gate

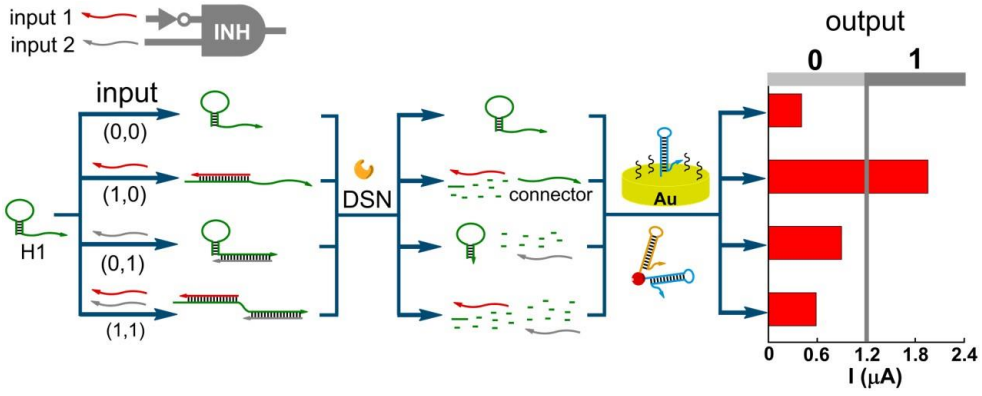

Figure S11. Construction of INH logic gate. The threshold is set as 1.2 μA.

Truth Tables.

AND gate

input		output
0	0	0
1	0	0
0	1	0
1	1	1

INH gate

input		output
0	0	0
1	0	1
0	1	0
1	1	0

Figure S12. The truth tables of AND and INH gates.

References

(S1) Fan, G.-C.; Ren, X.-L.; Zhu, C.; Zhang, J.-R.; Zhu, J.-J. *Biosens. Bioelectron.* **2014**, *59*, 45-53.

(S2) Li, S.; Xu, L.; Ma, W.; Wu, X.; Sun, M.; Kuang, H.; Wang, L.; A. Kotov, N.; Xu, C. *J. Am. Chem. Soc*. **2016**, *138*, 306-312.

(S3) Yin, B.-C.; Liu, Y.-Q.; Ye, B.-C. *J. Am. Chem. Soc.* **2012**, *134*, 5064-5067.

(S4) Zhang, J.; Wu, D.; Chen, Q.; Chen, M.; Xia, Y.; Cai, S.; Zhang, X.; Wu, F.; Chen, J. *Analyst* **2015**, *140*, 5082-5089.

(S5) Zhou, H.; Yang, C.; Chen, H.; Li, X.; Li, Y.; Fan, X. *Biosens.Bioelectron.* **2017**, *87*, 552-557.

(S6) Lin, X.; Zhang, C.; Huang, Y.; Zhu, Z.; Chen, X.; Yang, C. J. *Chem. Commun.* **2013**, *49*, 7243-7245.

(S7) Degliangeli, F.; Kshirsagar, P.; Brunetti, V.; Pompa, P. P.; Fiammengo, R. *J. Am. Chem. Soc.* **2014**, *136*, 2264-2267.

(S8) Shen, W.; Deng, H.; Ren, Y.; Gao, Z. *Chem. Commun.* **2013**, *49*, 4959-4961.

(S9) Ren, Y.; Deng, H.; Shen, W.; Gao, Z. *Anal. Chem.* **2013**, *85*, 4784-4789.

(S10) Yang, C.; Dou, B.; Shi, K.; Chai, Y.; Xiang, Y.; Yuan, R. *Anal*. *Chem*. **2014**, *86*, 11913-11918.

(S11) Hou, T.; Li, W.; Liu, X.; Li, F. *Anal*. *Chem*. **2015**, *87*, 11368-11374.

(S12) Wu, X.; Chai, Y.; Zhang, P.; Yuan, R. *ACS Appl*. *Mater*. *Interfaces* **2015**, *7*, 713-720.

(S13) Yang, C.; Shi, K.; Dou, B.; Xiang, Y.; Chai, Y.; Yuan, R. *ACS Appl*. *Mater*. *Interfaces* **2015**, *7*, 1188-1193.

(S14) Yu, Y.; Chen, Z.; Shi, L.; Yang, F.; Pan, J.; Zhang, B.; Sun, D. *Anal. Chem.* **2014**, *86*, 8200-8205.

(S15) Ge, L.; Wang, W.; Li, F. *Anal. Chem.* **2017**, *89*, 11560-11567.

(S16) Dong, Y.-P.; Wang, J.; Peng, Y.; Zhu, J.-J. *J. Electroanal. Chem.* **2016**, *781*, 109-113.

(S17) Mo, Y.-M.; Tang, Y.; Gao, F.; Yang, J.; Zhang, Y.-M. *Ind. Eng. Chem. Res.* **2012**, 51, 5995-6000.

(S18) Kulakovich, O.; Strekal, N.; Yaroshevich, A.; Maskevich, S.; Gaponenko, S.; Nabiev, I.; Woggon, U.; Artemyev, M. *Nano Lett.* **2002**, *2*, 1449-1452.

(S19) Ma, Z.-Y.; Ruan, Y.-F.; Xu, F.; Zhao, W.-W.; Xu, J.-J.; Chen, H.-Y. *Anal. Chem.* **2016**, *88*, 3864-3871.